Journal of Hazardous Materials 182 (2010) 665–671

Contents lists available at ScienceDirect

Journal of Hazardous Materials

journal homepage: www.elsevier.com/locate/jhazmat

# Effect of alkali cations on heterogeneous photo-Fenton process mediated by Prussian blue colloids

Shou-Qing Liu*, Shi Cheng, Lian-Rong Feng, Xiao-Mei Wang, Zhi-Gang Chen

*Provincial Key Laboratory of Environmental Science and Engineering, College of Chemistry and Bioengineering, Suzhou University of Science and Technology, Suzhou 215009, China*

ARTICLE INFO

*Article history:*
Received 26 March 2010
Received in revised form 14 June 2010
Accepted 20 June 2010
Available online 25 June 2010

*Keywords:*
Prussian blue
Heterogeneous catalysis
Photo-Fenton
Cation effect
Molecular recognition

ABSTRACT

This article evaluates Prussian blue (iron hexacyanoferrate) colloids as a heterogeneous photo-Fenton catalyst for the degradation of Rhodamine B. The emphasis is laid on the effects of alkali metal cations on the photo-Fenton process. The facts show that alkali cations strongly affect the degradation rate of organic species. The degradation rates of Rhodamine B, Malachite Green, and Methyl Orange in the presence of KCl, $KNO_3$, and $K_2SO_4$, respectively, are faster than their degradation rates in the presence of the corresponding sodium salts. The average degradation rates of Rhodamine B in 0.2 M KCl, NaCl, RbCl, and CsCl solution, decline in sequence, and the rate in KCl solution is greater than that without any salt added deliberately. Thus, potassium ions accelerate the degradation rate, but sodium, rubidium, and cesium ions slow the rate. The order of the rates is $R_K > R > R_{Na} > R_{Rb} > R_{Cs}$, which is consistent with that of the voltammetric oxidation currents of Prussian blue in the corresponding cation solutions. This phenomenon is attributed to the molecular recognition of the microstructure in Prussian blue nanoparticles to the alkali cations. The reaction mechanism of the photo-Fenton process has also been explored.



## 1. Introduction

The mixture of hydrogen peroxide and ferrous salts was called the Fenton reagent, as Fenton found that it oxidized tartaric acid in 1894 [1]. Subsequently, Haber and Weiss proposed that the hydroxyl radicals were the actual oxidants in the mixture of $H_2O_2 + Fe^{2+}$ and the proposal was confirmed by Merz and Waters [2]. Because the potential of the hydroxyl radicals was very high (2.84 V versus SHE), the Fenton reagent rapidly found its applications in eliminating the refractory organic contaminants in wastewater, and thereafter this reagent was developed into an advanced oxidation technology (AOT) in the treatment of non-biodegradable organic pollutants. Now it is well known that the Fenton process involves the reactions below [2–5].

$$Fe^{2+} + H_2O_2 \rightarrow Fe^{3+} + OH^- + {}^{\bullet}OH \qquad k_1 = 76\,M^{-1}\,s^{-1} \quad (1)$$

$$Fe^{3+} + H_2O_2 \rightarrow Fe^{2+} + H^+ + HOO^{\bullet} \qquad k_2 = 0.01\text{–}0.02\,M^{-1}\,s^{-1} \quad (2)$$

$$Fe^{3+} + HOO^{\bullet} \rightarrow Fe^{2+} + H^+ + O_2 \qquad k_3 = 1.2 \times 10^6\,M^{-1}\,s^{-1} \quad (3)$$

$$Fe^{2+} + {}^{\bullet}OH \rightarrow Fe^{3+} + OH^- \qquad k_4 = 3.2 \times 10^8\,M^{-1}\,s^{-1} \quad (4)$$

$$H_2O_2 + {}^{\bullet}OH \rightarrow H_2O + HOO^{\bullet} \qquad k_5 = 3.3 \times 10^7\,M^{-1}\,s^{-1} \quad (5)$$

$${}^{\bullet}OH + \text{organics} \rightarrow \text{intermediates} \rightarrow CO_2 + H_2O$$

$$k_6 = 10^7 - 10^{10}\,M^{-1}\,s^{-1} \quad (6)$$

Hydroxyl radicals could be formed by Eq. (1), thus the reaction cycle could proceed continuously if ferrous ions could be effectively regenerated (Eqs. (2) and (3)). However, ferrous ions are consumed more rapidly than they are regenerated because the rate constant $k_2$ was smaller than $k_1$ (Ferrous ions were also consumed by Eq. (4)) by comparison. In order to improve the Fenton process, Zepp et al. [5,6] developed the photo-Fenton system, in which UV irradiation was found to accelerate the overall process due to photochemical reactions reducing ferric ions into ferrous ions and splitting hydrogen peroxide (Eqs. (7)–(9))

$$[Fe(H_2O)]^{3+} + h\nu \rightarrow Fe^{2+} + {}^{\bullet}OH + H^+ \quad (7)$$

$$H_2O_2 + h\nu \rightarrow 2{}^{\bullet}OH \quad (8)$$

$$H_2O_2 + h\nu \rightarrow H^{\bullet} + HOO^{\bullet} \quad (9)$$

In addition, the effects of anions such as, $Cl^-$, $NO_3^-$, $SO_4^{2-}$, and $ClO_4^-$ on the Fenton reaction were also studied [7–12], and the effects were explained on the basis of the activities of the anion radicals, by comparison with those of the hydroxyl radicals. The optimal pH value for operations was found to be in the range of 2.8–3.3, which limited its application. To overcome the drawback the heterogeneous Fenton-like reagents were developed by immobilizing the ferrous or ferric ions on a carbon nanotube [13],

* Corresponding author. Tel.: +86 512 68056461; fax: +86 512 69209055.
*E-mail address:* shouqing_liu@hotmail.com (S.-Q. Liu).

0304-3894/$ – see front matter © 2010 Elsevier B.V. All rights reserved.
doi:10.1016/j.jhazmat.2010.06.083

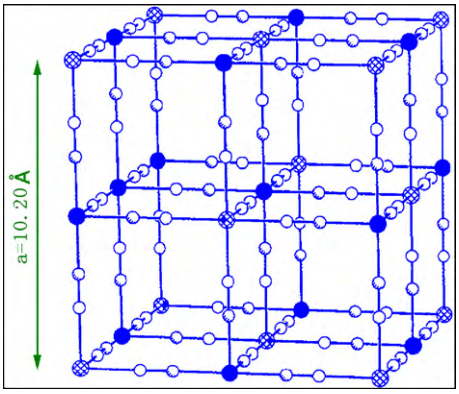


**Fig. 1.** Unit cell for the structure of Prussian blue. Cross-hatched spheres represent $Fe^{3+}$ ions; solid spheres represent $Fe^{2+}$ ions, hollow rings stand for carbon atoms, shade rings for nitrogen atoms; and water molecules and cations are omitted.

porous activated carbon [13–15], mesoporous silica [16,17], clay [18,19], and others [20–22]. The Fenton-like heterogeneous catalysts supported on the zeolite were studied in particular, broadly [23–29], due to the zeolitic porosity, stability, confinement effect, and adjustable channel size [30–32]. The investigations are of very great value in eliminating the organic pollutants and elucidating the principle of catalytic reactions.

From Eqs. (1)–(4) and (7) we can see that the Fenton or photo-Fenton reactions involve electron transfers and transformation of electrical states related to species, for example, metal iron ions. Therefore, the parameters that affect the rate of electron transfers, such as, the microstructure of heterogeneous catalysts and counter ions will have a great influence on the Fenton reaction rate. In fact, the microstructure of the heterogeneous catalysts has a strong impact on the reactivity and selectivity [33–35]. Unfortunately, the effects of the microstructure inside the heterogeneous catalysts and alkali cations (counter ions) on Fenton or on the photo-Fenton process have not received enough attention. Herein we use Prussian blue (PB) (similar to the zeolite in structure and features) as a model catalyst for exploring the effects of the microstructure of catalysts and focusing on the effects of alkali cations on the photo-Fenton degradation of the organic species, based on our previous study [36], where we reported the electrochemical behaviors of a self-assembled PB electrode [37] and its analog lanthanum hexacyanoferrate [38].

It is essential to know the microstructure of Prussian blue for the understanding the effects of cations on photo-Fenton reactions. Prussian blue (Iron$^{III}$ hexacyanoferrate$^{II}$) is the prototype transition metal hexacyanoferrate (MHCF), with a general formula of $A_hM_k[Fe(CN)_6]_l{\cdot}mH_2O$ ($h$, $k$, $l$, $m$ are stoichiometric numbers, A = alkali metal cation, M is $Fe^{2+}$, $Co^{2+}$, $Ni^{2+}$, $Cu^{2+}$, etc., transition metal ions) [39]. It is also the first coordination compound reported in scientific literature. The basic structure of Prussian blue is a three-dimensional polymeric network [40–42] with a face-centered cubic cell [40,43,44] consisting of alternating ferric (coordinated to nitrogen) and ferrous (coordinated to carbon atom) ions linked via the bridging cyanide ligands. The lattice constant of the unit cell is 10.20 Å (Fig. 1) and the diameter of the lattice channel is 3.2 Å [45], which accommodates water molecules and metal cations (countercations) to maintain electroneutrality. The countercations will penetrate into or flow out of the lattice channels of Prussian blue as denoted in Eqs. (10) and (11) with the electron transfers when the redox or electrochemical reactions occur as denoted below [46–48].

$$\underset{\text{Prussian blue}}{KFe^{III}Fe^{II}(CN)_6} - e = \underset{\text{Prussian yellow}}{Fe^{III}Fe^{III}(CN)_6} + K^+ \quad (10)$$

$$KFe^{III}Fe^{II}(CN)_6 + K^+ + e = \underset{\text{Prussian white}}{K_2Fe^{II}Fe^{II}(CN)_6} \quad (11)$$

It is seen that potassium ions will flow out the lattice channel of Prussian blue if it is oxidized (Eq. (10)), and potassium ions will enter into the lattice channel again when Prussian yellow is reduced. Prussian blue is also reduced directly to Prussian white (Eq. (11)) with the potassium ions immigrating the lattice channel. Therefore, the cation exchange reactions will take place when the oxidation states change. It is obvious that the cations with the match size could flow easily via the lattice channel.

## 2. Experimental

### 2.1. Materials

Rhodamine B (RhB), Malachite Green (MG), and Methyl Orange (MO) were purchased from Sigma. $(NH_4)_2Fe(SO_4)_2$, $K_3Fe(CN)_6$, KCl, NaCl, RbCl, CsCl, KBr, NaBr, $KNO_3$, $NaNO_3$, $K_2SO_4$, $N_2SO_4$ were of analytical grade and used as received. All solutions were prepared using 18.2 MΩ Milli-Q water.

### 2.2. Synthesis of Prussian blue

Prussian blue was synthesized by a mixture of equivalent amounts of $K_3Fe(CN)_6$ and $(NH_4)_2Fe(SO_4)_2$ aqueous solution. Generally, potassium ferricyanide 100 mL $2.0 \times 10^{-3}$ M and ammonium ferrous sulfate 100 mL $2.0 \times 10^{-3}$ M were mixed in a 500 mL flask, and PB colloid stock solution (200 mL $1.0 \times 10^{-3}$ M) was obtained for the photo-Fenton reaction.

### 2.3. Preparation of Prussian blue electrode and electrochemical characterization

A glassy carbon (GC) disk electrode of 3.0 mm diameter was used as the matrix of the working electrode. The GC electrode was polished by using a piece of 1200 diamond paper with 0.3–0.05 μm alumina by turns. Then the GC electrode was washed with absolute alcohol and distilled water in an ultrasonic bath for 5 min in turn. Thus a mirror-like, shiny electrode was obtained.

The obtained GC electrode was set up in a three-electrode system for cyclic voltammetric experiments.

The GC electrode obtained according to the above-mentioned method was immersed in the mixture of $1.0 \times 10^{-3}$ M $K_3Fe(CN)_6 + 1.0 \times 10^{-3}$ M $FeCl_3$ containing 0.2 M KCl, supporting the electrolyte for a cyclic voltammetric sweep for three cycles, in the potential range of −0.2 to 1.0 V at a scan rate of 100.0 mV $s^{-1}$. As a result, Prussian blue was immobilized on the surface of the GC electrode, and the as-prepared electrode was denoted as the PB-modified electrode.

The cyclic voltammetric (CV) experiments were carried out with a CHI660C electrochemical workstation (CH Instrument Company, Texas, USA) at room temperature (25 ± 2°C). All potentials were reported versus SCE.

### 2.4. Characterization for structure

Prussian blue powder was obtained by centrifugation and dried. First, the Prussian blue colloid solution was centrifuged in the presence of 0.2 M KCl, and then it was washed with 70% ethanol aqueous solution, and again centrifuged. The procedure was repeated thrice. The resulting precipitation was dried at 110 °C for three hours and collected for X-ray diffraction (XRD) measurement. The XRD measurement was conducted with X'Pert-Pro MPD X-ray diffractometer, Panalytical, Netherland. The source of the X-ray was Cu-K(, with a wavelength of 0.154 nm at a tube voltage of 40 kV, and a tube

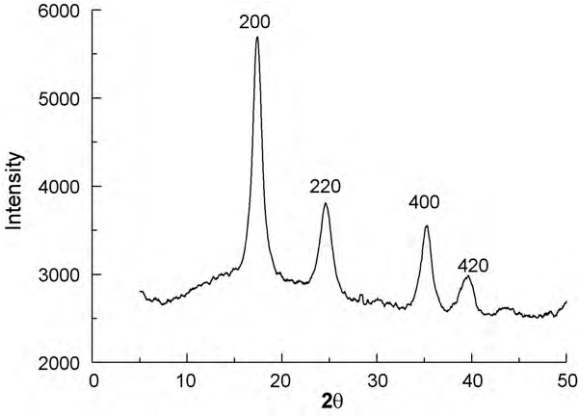


**Fig. 2.** Powder diffraction pattern of Prussian blue.

current of 40 mA. The morphological observation was carried out with a TecnaiG220 transmission electron microscope. A drop of the freshly prepared PB colloid solution was placed on carbon-coated copper grids and dried under ambient conditions for morphological observation.

### 2.5. Analytical methods

All photo-catalytic experiments were conducted under visible irradiation (( > 420 nm). A 300 W ultraviolet–visible lamp (OSRAM, Germany) was used as the irradiation source. The photo-Fenton degradation of organic compounds was performed in a 100 mL beaker. The distance between the lamp and the test solution was about 10 cm. The wall of the beaker was shielded with tinfoil from the surrounding light. The visible light was obtained with a ( > 420 nm cut-off filter, which covered the window of the beaker so that it could absorb the ultraviolet light and enable visible light of ( > 420 nm to pass. Generally, a 50 mL test solution was used in the photo-Fenton experiments. In the solution, the concentrations of hydrogen peroxide, PB, and organic compounds (RhB, MG, and MO) were adjusted according to the desired amount and the pH value of the mixed solution was about 6.0. The absorbance of RhB, MG, and MO in the photo-Fenton process was measured at regular intervals by a double beam TU-1901 spectrophotometer. The cyclic voltammetric (CV) experiments were carried out with a CHI660C electrochemical workstation (CH Instrument Company, Texas, USA) using a three-electrode system, at room temperature ($25 \pm 2\,^{\circ}C$). A glassy carbon disk electrode (diameter 3.0 mm) was used as the working electrode, a platinum sheet and a saturated calomel electrode (SCE) were used as the counter electrode and the reference electrode, respectively. All potentials were reported versus SCE.

## 3. Results and discussion

### 3.1. Characterization of Prussian blue heterogeneous catalyst

The measurement of the X-ray powder diffraction for the blue precipitate, synthesized according to the mentioned method, was performed and the diffraction pattern is shown in Fig. 2.

As shown in Fig. 2, the four major characteristic diffraction peaks at $2\theta = 17.55$, 24.62, 35.28, and 39.72 were corresponding to the (2 0 0), (2 2 0), (4 0 0), and (4 2 0) Bragg reflections at the $d$ spacings of 5.05 Å, 3.61 Å, 2.54 Å, and 2.27 Å, respectively. The positions of these diffraction peaks were in agreement with a face-centered cubic cell of Prussian blue with $a = 10.2$ Å [40,43,44], and also with JCPDS No.52-1907 in Table 1. The wide diffraction peaks suggested that the size of the as-prepared Prussian blue was in the nanometer

**Table 1**
Data of XRD for Prussian blue.

| | | | | | |
|---|---|---|---|---|---|
| PB | $2\theta$ (°) | 17.55 | 24.62 | 35.28 | 39.72 |
| | $d$ (A) | 5.05 | 3.61 | 2.54 | 2.27 |
| JCPDS 52-1907 | $d$ (A) | 5.10 | 3.60 | 2.55 | 2.28 |
| | $h\,k\,l$ | 200 | 220 | 400 | 420 |

range, the mean diameter of 33.8 nm has been calculated using the Debye–Scherrer formula

$$D = \frac{0.94\lambda}{\beta \cos\theta},$$

where $D$ is the crystal size, $\lambda$ is the wavelength of X-ray radiation (0.154 nm for Cu Kα radiation), $\beta$ is the full width at half-maximum, and $\theta$ is the diffraction angle [49]. It was in agreement with the TEM observation, the diameter of particles was distributed in the range from 30 nm to 50 nm shown in Fig. 3.

### 3.2. Effects of potassium and sodium ions

The Prussian blue formed according to the above-mentioned method was used as a heterogeneous photo-Fenton catalyst. RhB was degraded under ( > 420 nm visible irradiation in the presence of different potassium salts and the corresponding sodium salts under comparable conditions, respectively. The degradation curves are shown in Fig. 4.

By comparing the data in Fig. 4, it is seen that the degradation ratio of RhB in the case of potassium salts, at the same reaction time, is always greater than that in sodium salts in the same anion solutions (the degradation ratio of curve a is greater than that of curve b, and the one of curve c is greater than that of curve d in Fig. 4A and B), under comparable conditions. For example, the rate in the KCl system is faster than that in the NaCl system and the rate in the KBr system is also faster than that in NaBr system. Similarly, the degradation of MG and MO has been performed under comparable conditions. The results are listed in Table 2

It can be seen from Table 2 that the degradation ratio in the presence of KCl is 100.0%, while it is only 29.0% in the presence of NaCl, under similar conditions, for MG. Furthermore, the degradation ratios of MG or MO in the presence of KBr, $KNO_3$, and $K_2SO_4$ are all larger than those in the presence of the corresponding sodium bromide, nitrate, and sulfate, respectively. The degradation of the

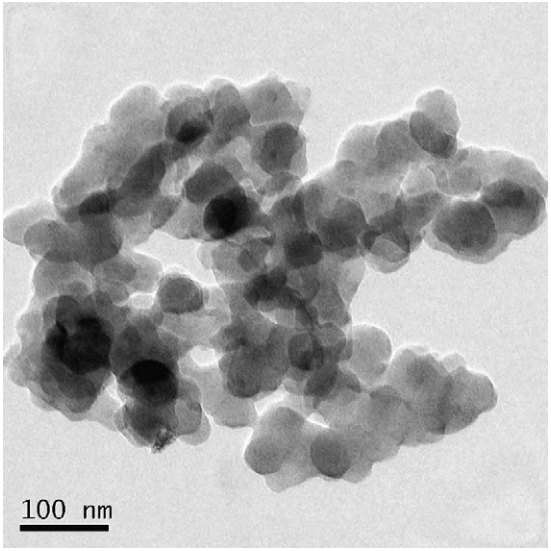


**Fig. 3.** TEM imagine of Prussian blue.

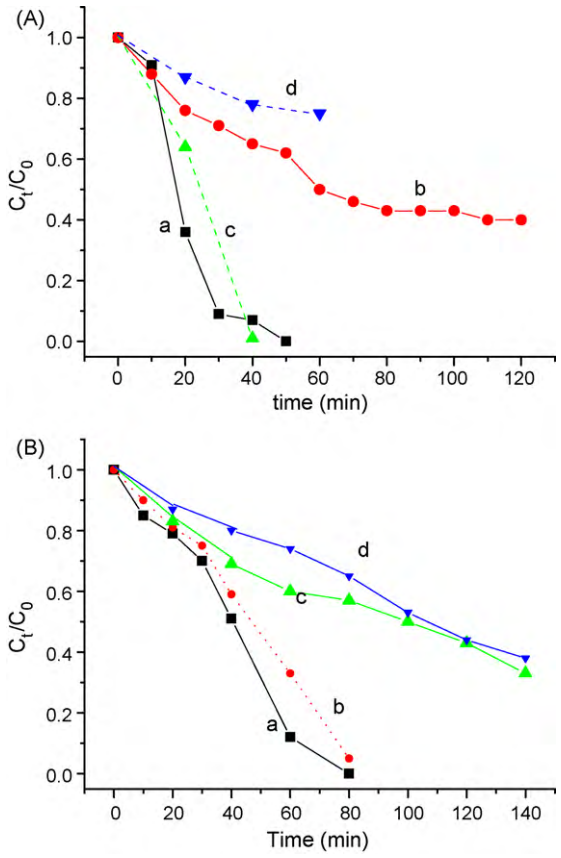


**Fig. 4.** (A) Curves a and b show the degradation of 4.8 mg $L^{-1}$ RhB (containing $2.0 \times 10^{-4}$ M PB + $2.0 \times 10^{-3}$ M $H_2O_2$) in 0.20 M KCl (a) and 0.20 M NaCl (b), respectively; Curves c and d show the degradation of 4.8 mg $L^{-1}$ RhB (containing $1.0 \times 10^{-4}$ M PB + $1.0 \times 10^{-3}$ M $H_2O_2$) in 0.50 M $KNO_3$ (c) and 0.50 M $NaNO_3$ (d), respectively. (B) Curves a and b show the degradation of 4.8 mg $L^{-1}$ RhB (containing $1.0 \times 10^{-4}$ M PB + $1.0 \times 10^{-3}$ M $H_2O_2$) in 0.50 M KBr (a) and 0.50 M NaBr (b), respectively; Curves c and d show the degradation of 4.8 mg $L^{-1}$ RhB (containing $2.0 \times 10^{-4}$ M PB + $2.0 \times 10^{-3}$ M $H_2O_2$) in 0.25 M $K_2SO_4$ (c) and 0.25 M $Na_2SO_4$ (d), respectively.

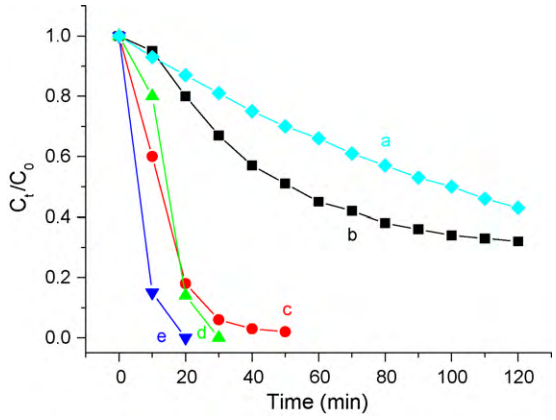


**Fig. 5.** Degradation curves of RhB at different concentrations of potassium chloride initial conditions: $1 \times 10^{-4}$ M PB + $1 \times 10^{-3}$ M $H_2O_2$ + 4.8 mg $L^{-1}$ RhB + KCl; (a) 0.0 M KCl; (b) 0.10 M KCl; (c) 0.25 M KCl; (d) 0.50 M KCl; and (e) 1.00 M KCl.

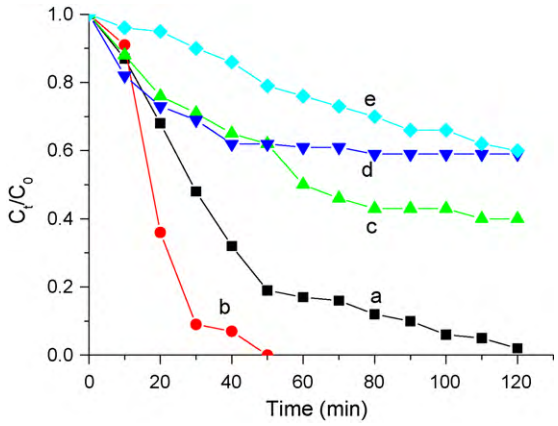


**Fig. 6.** Degradation curves of 4.8 mg $L^{-1}$ RhB containing $2 \times 10^{-4}$ M PB + $2 \times 10^{-3}$ M $H_2O_2$, (a) no salinity, (b) 0.2 M KCl added, (c) 0.2 M NaCl added, (d) 0.2 M RbCl added, and (e) 0.2 M CsCl added.

three organic compounds certainly shows that the cations have obvious effects on the degradation of organic compounds in the PB photo-Fenton system, and the degradation rates in the solutions containing potassium salts are always faster than those in the presence of the corresponding sodium salts. The effects of salts involve both cations used and the microstructure of Prussian blue. It was believed that the flux of cations in Prussian blue determines the decoloration rate of the dyes.

### 3.3. Effects of the concentration of potassium ions

According to the published literature, the chloride anions inhibit the degradation process in the organic species, because it is a scavenger of the hydroxyl radicals [9–13]. Interestingly, the addition of KCl (but not NaCl) can promote the photo-Fenton process in the PB system. It can be seen from the degradation curves (Fig. 5) at the different concentrations of KCl that the times for the ratio of $C_t/C_0$ ($C_0$ is the initial concentration of organic compounds, $C_t$ is the concentration that has not been degraded) reaching zero are 50 min, 30 min, and 20 min at concentrations of 0.25 M, 0.50 M, and 1.00 M KCl, respectively. The order of the degradation rates is $R_{1.00} > R_{0.50} > R_{0.25} > R_{0.10} > R_{0.00}$. This clearly shows that the degradation rate increases as the concentration of KCl increases. It also confirms that the potassium cations affect the reaction process. It is believed that it is the potassium ions that accelerate the photo-Fenton process, because chloride anions, as mentioned, are scavengers of the hydroxyl radicals.

### 3.4. Comparison of alkali metal ions and electrochemical evidence

Further studies show that the photo-Fenton decoloration ratio of RhB in the PB system, in the presence of the same concentration of 0.2 M KCl, NaCl, RbCl, and CsCl, respectively, is different from each

**Table 2**
Degradation ratios of MG and MO in the presence of potassium and sodium salts*.

| | Chlorides | | Bromides | | Nitrates | | Sulfates | |
|---|---|---|---|---|---|---|---|---|
| | KCl | NaCl | KBr | NaBr | $KNO_3$ | $NaNO_3$ | $K_2SO_4$ | $Na_2SO_4$ |
| MG | 100.0%(a) | 29.0%(a) | 97.0%(b) | 89.0%(b) | 61.0%(c) | 32.0%(c) | 74.0%(d) | 59.0%(d) |
| MO | 100.0%(e) | 5.0%(e) | 83.0%(f) | 64.0%(f) | 93.0%(g) | 49.0%(g) | 76.0%(h) | 53.0%(h) |

* Initial conditions: The reaction system contained $1 \times 10^{-4}$ M PB + $1 \times 10^{-3}$ M $H_2O_2$ + 0.5 M salt + 10 mg $L^{-1}$ MG or MO. The photo-Fenton reaction times were 30 min (a), 60 min (b), 120 min (c), 180 min (d), 40 min (e, f), 240 min (g), and 270 min (h), respectively. The concentration of sulfates was 0.25 M (d, h).

**Table 3**
Decoloration ratio and average degradation rate of RhB in the presence of different alkali cations (0.20 M) at 80 min.

| Alkali cations | No salinity | KCl[a] | NaCl | RbCl | CsCl |
|---|---|---|---|---|---|
| Decoloration ratio (%) | 88.0 | 100 | 57.2 | 41.2 | 30.1 |
| Average rate (mg $L^{-1}$ $min^{-1}$) | 0.054 | 0.096 | 0.034 | 0.025 | 0.018 |

[a] The reaction was completed in 50 min.

other (see Fig. 6). The decoloration ratio and average reaction rate at 80 min in the presence of alkali cations are listed in Table 3. It is seen that the order of the decoloration rates is $R_{KCl} \gg R_{NaCl} > R_{RbCl} > R_{CsCl}$. In fact, the addition of KCl promotes the degradation reaction, while the presence of NaCl, RbCl, and CsCl restrains the reaction rate by comparison.

The effects of salts involve both cations used and the microstructure of Prussian blue. The electrochemical studies have shown that the move of cations in the channel of Prussian blue determines the electron-transfer rate [46,50,51] because cations will move in or out of the channels of Prussian blue to maintain the electroneutrality when the electron-transfer reactions take place as denoted Eqs. (10) and (11). Our experimental results also confirm the current order is $I_{K+} > I_{Na+} > I_{Rb+} > I_{Cs+}$ for the oxidation of the PB electrode in the alkali cation solutions (Fig. 7), which is consistent with that reported in literature [46,50,51].

Since both the electrochemical process and photo-Fenton process involve the electron-transfer reactions, the parameters affecting the rate of electron transfers in the electrochemical process, such as the size of the countercations, will also play a major role in the photo-Fenton process in the PB system.

As mentioned, Prussian blue has zeolite-like features that function as molecular sieves, therefore, the selective ion transfers can elucidate both the electrochemical reaction rate and photo-Fenton reaction in terms of hydrated ionic radii and the channel radius of the lattice in Prussian blue. The channel radius of Prussian blue is 1.60 Å. Thus, only a few countercations with the hydrated radii smaller than the channel size in PB can move through the channel lattices. Potassium ions with 1.25 Å [46,51] of the hydrated radius, which are smaller than 1.60 Å of the lattice radius in the PB structure, can move freely through the lattice channel of PB, hence, they cause the largest oxidation current in electrochemistry, and the corresponding greatest degradation rate in the photo-Fenton process can be observed. Sodium ions with a hydrated radius of 1.83 Å find it difficult to move in or out. Only the partial dehydrated ions can penetrate through the lattice, leading to a small electrochemical current peak [51,52] and a low rate of photo-Fenton degradation, compared to that in the KCl system. In the case of the small hydrated cations (1.18 Å for $Rb^+$ and 1.19 Å for $Cs^+$), the cation-induced microstructural distortion can be a mass-transfer and rate-determining factor [48,51], which results in very slow motions of both $Rb^+$ and $Cs^+$ in the lattice channel of PB, thus very low currents are observed in Fig. 7, and the corresponding photo-Fenton rates are also very small. In summary, the recognition of the lattice size of Prussian blue to alkali cations determines the mobility of alkali cations in the lattice, which in turn plays a pivotal role in the PB photo-Fenton process.

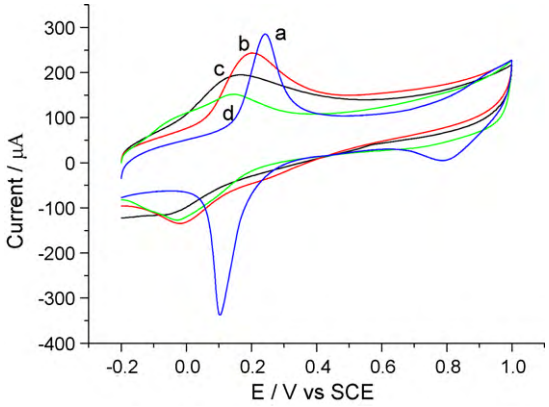


**Fig. 7.** Cyclic voltammetric responses of a PB-modified electrode in the potential of −0.2 to 1.0 V, at the scan rate of 0.1 V $s^{-1}$ in (a) 0.2 M KCl, (b) 0.2 M NaCl, (c) 0.2 M RbCl, and (d) 0.2 M CsCl supporting electrolyte, respectively.

### 3.5. Analysis of the reaction mechanism

Analysis of the reaction mechanism of the photo-Fenton process is based on the three basic facts mentioned herewith: The first one is that the cations in the PB system strongly affect the rate of the photo-Fenton process, suggesting that the photo-catalytic reactions take place not only on the surface of the PB particles, but also inside the PB particles; Second, it has been conclusively shown [53,54] that the electron-transfer reactions observed at about 0.2 V versus SCE are assigned to the high-spin iron ($Fe^{III}$, coordinated to nitrogen) and 1.0 V versus SCE to the low-spin iron ($Fe^{II}$, coordinated to carbon) ions [55], respectively. Finally, it has been commonly accepted that the photodriven charge-transfer reaction for Prussian blue under irradiation is the intervalence charge-transfer reaction [54,43,56,57], denoted as follows

$$[K^+–Fe^{III}–(NC)_6–Fe^{II}] \xrightarrow{h\nu} [K^+–Fe^{II}–(NC)_6–Fe^{III}]^* \quad (12)$$

Consequently, Eq. (12) is the initial reaction of the photo-Fenton process in the PB system. Furthermore, $[K–Fe^{II}–(NC)_6–Fe^{III}]^*$ can oxidize hydrogen peroxide to release dioxygen, because the excited PB nanoparticles are metastable [57]. These metastable $Fe^{III}$ ions that coordinate with the carbon atoms have a high potential. For example, the open-circuit potential of $Fe^{III}Fe^{III}(CN)_6$ reaches 0.98 V versus SCE (1.22 V versus SHE) [45], while the standard electrode potential for $O_2/H_2O_2$ is 0.68 V. Our previous research has shown that the mixture of $Fe^{III}Fe^{III}(CN)_6 + H_2O_2$ in the presence of KCl results in $KFe^{III}Fe^{II}(CN)_6$ [37], indicating that the stable state of iron that coordinates with the carbon atom is the ferrous ion, while the ferric ion is unstable and has powerful oxidation. On the basis of these facts the second step reaction can be deduced as Eq. (11)

$$[K^+–Fe^{II}–(NC)_6–Fe^{III}]^* + H_2O_2 + K^+ \rightarrow [K_2{}^+–Fe^{II}–(NC)_6–Fe^{II}] + O_2 + 2H^+ \quad (13)$$

As a result, the potassium ions penetrate into the PB particles as countercations, to maintain the electroneutrality. One of the products of reaction (13), Prussian white $[K_2–Fe^{II}–(NC)_6–Fe^{II}]$, being in the reduced state, similar to the ferrous ions in Eq. (1), can transform hydrogen peroxide into hydroxyl radicals as shown in Eq. (14)

$$[K_2{}^+–Fe^{II}–(NC)_6–Fe^{II}] + H_2O_2 \rightarrow [K^+–Fe^{II}–(NC)_6–Fe^{III}] + K^+ + HO^\bullet + OH^- \quad (14)$$

It is seen that Prussian blue forms again; it returns to the starting reactant of Eq. (12). The catalytic reaction cycle involves potassium ions penetrating into and flowing out of the PB nanoparticles;

the faster the degradation rate, the greater is the concentration of potassium salts. It is reasonable that hydrogen peroxide inserts in the lattice channel of PB because a molecule of hydrogen peroxide occupies 2.42 Å [57], which is less than 3.2 Å for the diameter of PB channel. The mobility of alkali cations determines the degradation rate of organic compounds during the photo-Fenton process. (lines 50–59, page 10)

## 4. Conclusion

The mixture of Prussian blue and hydrogen peroxide can function as a heterogeneous Fenton reagent. This Fenton-like reagent can degrade organic pollutants. Alkali metal ions in the reaction systems can strongly affect the degradation rate, due to the molecular recognition of the lattice channel of Prussian blue to alkali cations. The phenomenon that potassium ions promote the photo-Fenton process, while sodium, rubidium, and cesium cations decline the process is the inevitable result of the selective recognition of Prussian blue. The result of this research is very useful for the design of heterogeneous Fenton-like catalysts supported on porous zeolites, because the zeolites have the function of molecular recognition like Prussian blue.

## Acknowledgements

This study was financially supported by the National Natural Science Foundation of China (No. 50973077, No. 20771047), Ministry of Housing and Urban-Rural Development of China (Grant: 06-K4-26), Provincial Key Laboratory of Environmental Science and Engineering, Jiangsu of China (Grant: 2D051204), the Creative Project of Postgraduate of Jiangsu Province (No. CX09S-049Z), and the Project from the Suzhou Environmental Protection Bureau, China. We also thank Mr. Xian-He Liu from the Huaqiao University of China for the language check and Dr. Huang for the electroscope support of Public Center for Characterization and Test, Suzhou Institute of Nano-tech and Nano-bionics, Chinese Academy of Sciences.

## References

[1] H.J.H. Fenton, Oxidation of tartaric acid in the presence of iron, J. Chem. Soc. 65 (1894) 899–911.
[2] C. Walling, Fenton's reagent revisited, Acc. Chem. Res. 8 (1975) 125–131.
[3] E. Neyens, J. Baeyens, A review of classic Fenton's peroxidation as an advanced oxidation technique, J. Hazard. Mater. B 98 (2003) 33–50.
[4] N. Masomboon, C. Ratanatamskul, M.C. Lu, Chemical oxidation of 2,6-dimethylaniline in the Fenton process, Environ. Sci. Technol. 43 (2009) 8629–8634.
[5] R.G. Zepp, B.C. Faust, J. Hoigné, Hydroxyl radical formation in aqueous reactions (pH 3–8) of iroin (II) with hydrogen peroxide: the photo-fenton reaction, J. Environ. Sci. Technol. 26 (1992) 313–319.
[6] E. Brillas, I. Sirés, M.A. Oturan, Electro-Fenton process and related electrochemical technologies based on Fenton's reaction chemistry, Chem. Rev. 109 (2009) 6570–6631.
[7] J.E.F. Moraes, F.H. Quina, C.A.O. Nascimento, D.N. Silva, O. Chiavone-Filho, Treatment of saline wastewater contaminated with hydrocarbons by the photo-Fenton process, Environ. Sci. Technol. 38 (2004) 1183–1187.
[8] J. Kiwi, A. Lopez, V. Nadtochenko, Mechanism and kinetics of the OH-radical intervention during Fenton oxidation in the presence of a significant amount of radical scavenger ($Cl^-$), Environ. Sci. Technol. 34 (2000) 2162–2168.
[9] J. Bacardit, J. Stötzner, E. Chamarro, S. Esplugas, Effect of salinity on photo-Fenton process, Ind. Eng. Chem. Res. 46 (2007) 7615–7619.
[10] J. Malešic, M. Strlic, J. Kolar, S. Polanc, The influence of halide and pseudo-halide antioxidants in Fenton-like reaction systems containing copper(II) ions, J. Mol. Catal. A: Chem. 241 (2005) 126–132.
[11] A. Machulek Jr., J.E.F. Moraes, C. Vautier-Giongo, C.A. Silverio, L.C. Friedrich, C.A.O. Nascimento, M.C. Gonzalez, F.H. Quina, Abatement of the inhibitory effect of chloride anions on the photo-Fenton process, Environ. Sci. Technol. 41 (2007) 8459–8463.
[12] R. Maciel, G.L. Sant'Anna Jr., M. Dezotti, Phenol removal from high salinity effluents using Fenton's regent and photo-Fenton reactions, Chemosphere 57 (2004) 711–719.
[13] A. Rodríguez, G. Ovejero, J.L. Sotelo, M. Mestanza, J. Garcí, Heterogeneous Fenton catalyst supports screening for mono azo dye degradation in contaminated wastewaters, Ind. Eng. Chem. Res. 49 (2010) 498–505.
[14] E. Kan, S.G. Huling, Effects of temperature and acidic pre-treatment on Fenton-driven oxidation of MTBE-spent granular activated carbon, Environ. Sci. Technol. 43 (2009) 1493–1499.
[15] J.H. Ramirez, F.J. Maldonado-Hodar, A.F. Perez-Cadenas, Azo-dye orange II degradation by heterogeneous Fenton-like reaction using carbon–Fe catalysts, Appl. Catal. B: Environ. 75 (2007) 312–323.
[16] G. Calleja, J.A. Melero, F. Martinez, R. Molina, Activity and resistance of iron-containing amorphous, zeolitic and mesostructured materials forwet peroxide oxidation of phenol, Water Res. 39 (2005) 1741–1750.
[17] F Martinez, G. Calleja, J.A. Melero, R. Molina, Iron species incorporated over different silica supports for the heterogeneous photo-Fenton oxidation of phenol, Appl. Catal. B: Environ. 70 (2007) 452–460.
[18] J. Feng, X. Hu, P.L. Yue, Novel bentonite clay-based Fe-nanocomposite as a heterogeneous catalyst for photo-Fenton discoloration and mineralization of orange II, Environ. Sci. Technol. 38 (2004) 269–275.
[19] J. Chen, L. Zhu, Heterogeneous UV-Fenton catalytic degradation of dyestuff in water with hydroxyl-Fe pillared bentonite, Catal. Today 126 (2007) 463–470.
[20] I. Muthuvel, M. Swaminathan, Highly solar active Fe(III) immobilised alumina for the degradation of acid violet 7, Sol. Energy Mater. Sol. Cells 92 (2008) 857–863.
[21] S. Parra, L. Henao, E. Mielczarski, J. Mielczarski, P. Albers, E. Suvorova, J. Guindet, J. Kiwi, Synthesis, testing, and characterization of a novel nafion membrane with superior performance in photoassisted immobilized Fenton catalysis, Langmuir 20 (2004) 5621–5629.
[22] Q Wang, E.M. Scherer, A.T. Lemley, Metribuzin degradation by membrane anodic Fenton treatment and its interaction with ferric ion, Environ. Sci. Technol. 38 (2004) 1221–1227.
[23] T.A. Ruda, P.K. Dutta, Fenton chemistry of $Fe^{III}$-exchanged eeolitic minerals treated with antioxidants, Environ. Sci. Technol. 39 (2005) 6147–6615.
[24] M.B. Kasiri, H. Aleboyeh, A. Aleboyeh, Degradation of acid blue 74 using Fe-ZSM5 zeolite as a heterogeneous photo-Fenton catalyst, Appl. Catal. B: Environ. 25 (2008) 1–15.
[25] F. Chen, Y. Li, W. Cai, J. Zhang, Preparation and sono-Fenton performance of 4A-zeolite supported-Fe2O3, J. Hazard. Mater. (2010), doi:10.1016/j.jhazmat.2009.12.094.
[26] M. Tekbas, H.C. Yatmaz, N. Bektas, Heterogeneous photo-Fenton oxidation of reactive azo dye solutions using iron exchanged zeolite as a catalyst, Micropor. Mesopor. Mater. 115 (2008) 594–602.
[27] R. Gonzalez-Olmos, U. Roland, H. Toufar, F.-D. Kopinke, Fe-zeolites as catalysts for chemical oxidation of MTBE in water with $H_2O_2$, A. Georgi, Appl. Catal. B: Environ. 89 (2009) 356–364.
[28] E.V. Parkhomchuk (Kuznetsova), M.P. Vanina, S. Preis, The activation of heterogeneous Fenton-type catalyst Fe-MFI, Catal. Commun. 9 (2008) 381–385.
[29] S. Wang, Z.H. Zhu, Characterisation and environmental application of an Australian natural zeolite for basic dye removal from aqueous solution, J. Hazard. Mater. B 136 (2006) 946–952.
[30] P.K. Dutta, Y. Kim, Photochemical processes in zeolites: new developments, Curr. Opin. Solid State Mater. Sci. 7 (2003) 483–490.
[31] S. Hashimoto, Zeolite photochemistry: impact of zeolites on photochemistry and feedback from photochemistry to zeolite science, J. Photochem. Photobiol. C: Photochem. Rev. 4 (2003) 19–49.
[32] A. Corma, State of the art and future challenges of zeolites as catalysts, J. Catal. 216 (2003) 298–312.
[33] G.A. Somorjai, J.Y. Park, Molecular factors of catalytic selectivity, Angew. Chem. Int. Ed. 47 (2008) 9212–9228.
[34] A. Bhan, E. Iglesia, A link between reactivity and local structure in acid catalysis on zeolites, Acc. Chem. Res. 41 (2008) 559–567.
[35] K.T. Ishihara, Y. Kamiya, T. Okuhara, S. Yamanaka, Water-Tolerant, Highly active solid acid catalysts composed of the Keggin-type polyoxometalate H3PW12O40 immobilized in hydrophobic nanospaces of organomodified mesoporous silica, Angew. Chem. Int. Ed. 46 (2007) 7625–7628.
[36] S. Liu, S. Cheng, L. Luo, H. Cheng, S. Wang, S. Lou, Degradation of dye rhodamine B under visible irradiation with Prussian blue as a photo-Fenton reagent, Environ. Chem. Lett. (2009), doi:10.1007/s10311-009-0242-x.
[37] S. Liu, J. Xu, H. Chen, Electrochemical behavior of nanosized Prussian blue self-assembled on Au electrode surface, Electrochem. Commun. 4 (2002) 421–425.
[38] S. Liu, H. Chen, Spectroscopic and voltammetric studies on a lanthanum hexacyanoferrate modified electrode, J. Electroanal. Chem. 528 (2002) 190–195.
[39] N.R. de Tacconi, K. Rajeshwar, Metal hexacyanoferrates: electrosynthesis, in situ characterization, and applications, Chem. Mater. 15 (2003) 3046–3062.
[40] F. Herren, P. Fischer, A. Ludi, W. Hälg, Neutron diffraction study of Prussian blue, $Fe_4[Fe(CN)_6]_3 \cdot xH_2O$. Location of water molecules and long-range magnetic order, Inorg. Chem. 19 (1980) 956–959.
[41] D. Ellis, M. Eckhoff, V.D. Neff, Electrochromism in the mixed-valence hexacyanides. 1. Voltammetric and spectral studies of the oxidation and reduction of thin films of Prussian blue, J. Phys. Chem. 85 (1981) 1225–1231.
[42] X. Zheng, Q. Kuang, T. Xu, Z. Jiang, S. Zhang, Z. Xie, R. Huang, L. Zheng, Growth of Prussian blue microcubes under a hydrothermal condition: possible nonclassical crystallization by a mesoscale self-Assembly, J. Phys. Chem. C 111 (2007) 4499–4502.
[43] M.B. Robin, The color and electronic configurations of Prussian blue, Inorg. Chem. 1 (1962) 337–342.
[44] Y. Ding, Y. Hu, G. Gu, X. Xia, Controllable synthesis and formation mechanism investigation of Prussian blue nanocrystals by using the polysaccharide hydrolysis method, J. Phys. Chem. C 113 (2009) 14838–14843.

[45] K. Itaya, T. Ataka, S. Toshima, Spectroelectrochemistry and electrochemical preparation method of Prussian blue modified electrodes, J. Am. Chem. Soc. 104 (1982) 4767–4772.
[46] J.J. García-Jareño, D. Giménez-Romero, F. Vicente, C. Gabrielli, M. Keddam, H. Perrot, EIS and Ac-electrogravimetry study of PB films in KCl, NaCl, and CsCl aqueous solutions, J. Phys. Chem. B 107 (2003) 11321–11330.
[47] H. Kahlert, Š. Komorsky-Lovric, M. Hermes, F. Scholz, A Prussian blue-based reactive electrode for the determination of thallium ions, Fresenius, J. Anal. Chem. 356 (1996) 204–208.
[48] A. Dostal, G. Kauschka, S.J. Reddy, F. Scholz, Lattice contractions and expansions accompanying the electrochemical conversions of Prussian blue and the reversible and irreversible insertion of rubidium and thallium ions, J. Electroanal. Chem. 406 (1996) 155–163.
[49] H.P. Klug, L.E. Alexander, X-ray Diffraction Procedures for Polycrystalline and Amorphous Materials, second ed., John Wiley & Sons, New York, 1974, p. 618.
[50] C.A. Lundgren, R.W. Murray, Observations on the composition of Prussian blue films and their electrochemistry, Inorg. Chem. 27 (1988) 933–939.
[51] M.H. Pournaghi-Azar, H. Dastangoo, Palladized aluminum as a novel substrate for the non-electrolytic preparation of a Prussian blue film modified electrode, J. Electroanal. Chem. 573 (2004) 355–364.
[52] M.A. Malik, K. Miecznikowski, P.J. Kulesza, Quartz crystal microbalance monitoring of mass transport during redox processes of cyanometallate modified electrodes: complex charge transport in nickel hexacyanoferrate films, Electrochim. Acta 45 (2000) 3777–3784.
[53] K. Itaya, T. Ataka, S. Toshima, T. Shinohara, Electrochemistry of Prussian blue. An in situ moessbauer effect measurement, J. Phys. Chem. 86 (1982) 2415–2418.
[54] K. Itaya, I. Uchida, Nature of intervalence charge-transfer bands in Prussian blues, Inorg. Chem. 25 (1986) 389–392.
[55] H. Vahrenkamp, A. Geib, G.N. Richardson, Cyanide-bridged oligonuclear complexes: features and attractions, J. Chem. Soc., Dalton Trans. 20 (1997) 3643–3651.
[56] M. Nihei, M. Ui, N. Hoshino, H. Oshio, Cyanide-bridged Iron (II, III) cube with multistepped redox behavior, Inorg. Chem. 47 (2008) 6106–6108;
A. Bleuzen, V. Marvaud, C. Mathoniere, B. Sieklucka, M. Verdaguer, Photomagnetism in clusters and extended molecule-based magnets, Inorg. Chem. 48 (2009) 3453–3466.
[57] E. Fois, A. Gamba, E. Spanoó, Competition between water and hydrogen peroxide at Ti center in titanium zeolites. An ab initio study, J. Phys. Chem. B. 108 (28) (2004) 9557–9560.